Journal of Hydrology: Regional Studies 42 (2022) 101175

Contents lists available at ScienceDirect

Journal of Hydrology: Regional Studies

journal homepage: www.elsevier.com/locate/ejrh

Climate change and the response of streamflow of watersheds under the high emission scenario in Lake Tana sub-basin, upper Blue Nile basin, Ethiopia

Gashaw Gismu Chakilu [a,*], Szegedi Sándor [b], Túri Zoltán [c], Kwanele Phinzi [d]

[a] Doctoral School of Earth Sciences, Department of Meteorology, University of Debrecen, Egyetem tér 1, 4032 Debrecen, Hungary
[b] Department of Meteorology, University of Debrecen, Egyetem tér 1, 4032 Debrecen, Hungary
[c] Department of Physical Geography and Geoinformatics, University of Debrecen, Egyetem tér 1, 4032 Debrecen, Hungary
[d] Doctoral School of Earth Sciences, Department of Physical Geography and Geoinformatics, University of Debrecen, Egyetem tér 1, 4032 Debrecen, Hungary

ARTICLE INFO

Keywords:
Climate change
Stream flow
SWAT
Lake Tana sub-basin
Upper Blue Nile basin

ABSTRACT

Study region: Lake Tana sub-basin, Upper Blue Nile basin, Ethiopia.
Study focuses: This study evaluated the degree to which climate is changing in the region, and its impact on stream flow of watersheds simulated by Soil Water Assessment Tool (SWAT) under the Representative Concentration Pathway (RCP8.5) emission scenario using six climate models including CanESM2, EC-EARTH, CNRM-CM5, HadGEM2- ES, NORESM1-M, and CSIRO-Mk3–6–0 by comparing the last thirty years of the past century (1971–2000) and the same years of this century (2071–2100). Bias correction for maximum temperature, minimum temperature, and rainfall data obtained from all climate models have been done using CMhyd software. The SWAT model is calibrated and validated using eleven sensitive hydrological parameters.
New hydrological insights: The result revealed that the change in maximum temperature ranges from 2.93 °C (November) and 5.17 °C (March), and the change in minimum temperature also ranges from 3.08 °C to 4.79 °C on a monthly basis. Rainfall is expected to increase up to 29.75% (November) and decrease up to 9.26% (March) in different seasons. Due to the change in climate, a flow is predicted to increase up to 27.82%, 27.47%, 26.47%, and 24.97% in Ribb, Gilgel Abay, Gumara, and Megech watersheds, respectively, and it is also decreasing in winter and spring seasons. On average, the streamflow is expected to increase by 5.89%, 5.63%, 4.92%, and 4.87% in Ribb, Gumara, Megech, and Gilgel Abay watersheds, respectively.

1. Introduction

Climate change is arguably the most important environmental challenge facing the world in the 21st century owing to its wide-reaching impacts on human society (Fulco et al., 2007). Although climate change is a naturally occurring phenomenon (US EPA, 2016), there is now a common consensus among the scientific community that anthropogenic activities are largely responsible for its occurrence, mainly through burning fossil fuels like oil, coal, and gas, leading to emissions of greenhouse gases (GHGs) to the

* Corresponding author.
E-mail addresses: gashaw.gismu@science.unideb.hu (G.G. Chakilu), szegedi.sandor@science.unideb.hu (S. Sándor), turi.zoltan@science.unideb.hu (T. Zoltán), kwanele.phinzi@science.unideb.hu (K. Phinzi).

https://doi.org/10.1016/j.ejrh.2022.101175
Received 8 March 2022; Received in revised form 8 July 2022; Accepted 11 July 2022
Available online 18 July 2022
2214-5818/

atmosphere (Henderson and Reinert, 2016). Until the 1800 s, the emission of these GHGs was relatively stable but has since continuously increased due to industrialization, population growth, and the subsequent increase in energy consumption, deforestation, and human settlements (North, 2014). During the past 15–20 years, the growth rate in heat-trapping GHGs emissions increased from 1.5 to 2 ppm per year (Hayhoe et al., 2017). Consequently, the global mean surface temperature for the decade 2006–2015 increased by 0.87 °C which is higher than the observed long-term average in the pre-industrial period (1850–1900) (IPCC, 2018). Due to the future anthropogenic activities and the emission of GHGs being uncertain, it is strongly believed that future global temperatures will keep changing. The Representative Concentration Pathways (RCPs), which are used for making projections based on these anthropogenic factors, describe four different pathways of GHG emissions and atmospheric concentrations, air pollutant emissions, and land use, in terms of a stringent mitigation scenario (RCP2.6), two intermediate scenarios (RCP4.5 and RCP6.0), and one scenario with very high GHG emissions (RCP8.5) that assumes radiative forcing concentration will reach 8.5 W/m^2 in the atmosphere and temperature increases up to 2.6–4.8°Cin the end of 21 st century (IPCC, 2014).

Over the past few decades, a plethora of climate models has been used to estimate the future climate of the earth under different scenarios. The annual values projected for precipitation by such models are inherently uncertain and often inconsistent because each model is slightly different (Tebaldi et al., 2011; Power et al., 2012; FAO, 2010; Schaller et al., 2011). However, the trend and magnitude of change in precipitation are fairly consistent among the models, most of which, revealed an increasing trend in heavy rainfall extremes towards the end of the 21st century almost in all parts of the world (Poveda and Martínez, 2011; Suppiah et al., 2013). Further projections show that the precipitation is very likely to increase in high latitudes and near major convergence zones in the tropics in some seasons, while decreases are expected in many subtropical regions (Stocker et al., 2013). Such changes in the intensity and distribution of precipitation will have serious implications on water (Seager et al., 2007; Sivakumar, 2011; Stoll et al., 2011), a key resource for economic growth and social development. Currently, approximately one-third of the world's population lives in water-stress countries, and by 2025, two-thirds of the world's population will experience water scarcity problems due to the reduction of river flow and groundwater recharge (FAO, 2010).

Due to climate change, more frequent severe droughts and flood events are expected to intensify in different regions (US EPA, 2016). In Ethiopia, over the past five decades, changes in rainfall and temperature have affected the various components of the hydrological cycle in major river basins (Gebremicael et al., 2013; Tesemma et al., 2010). In the country, the hydrological drought during dry seasons and flooding in rainy seasons have become a common problem in many perennial rivers as noted by (Bekele et al., 2021;

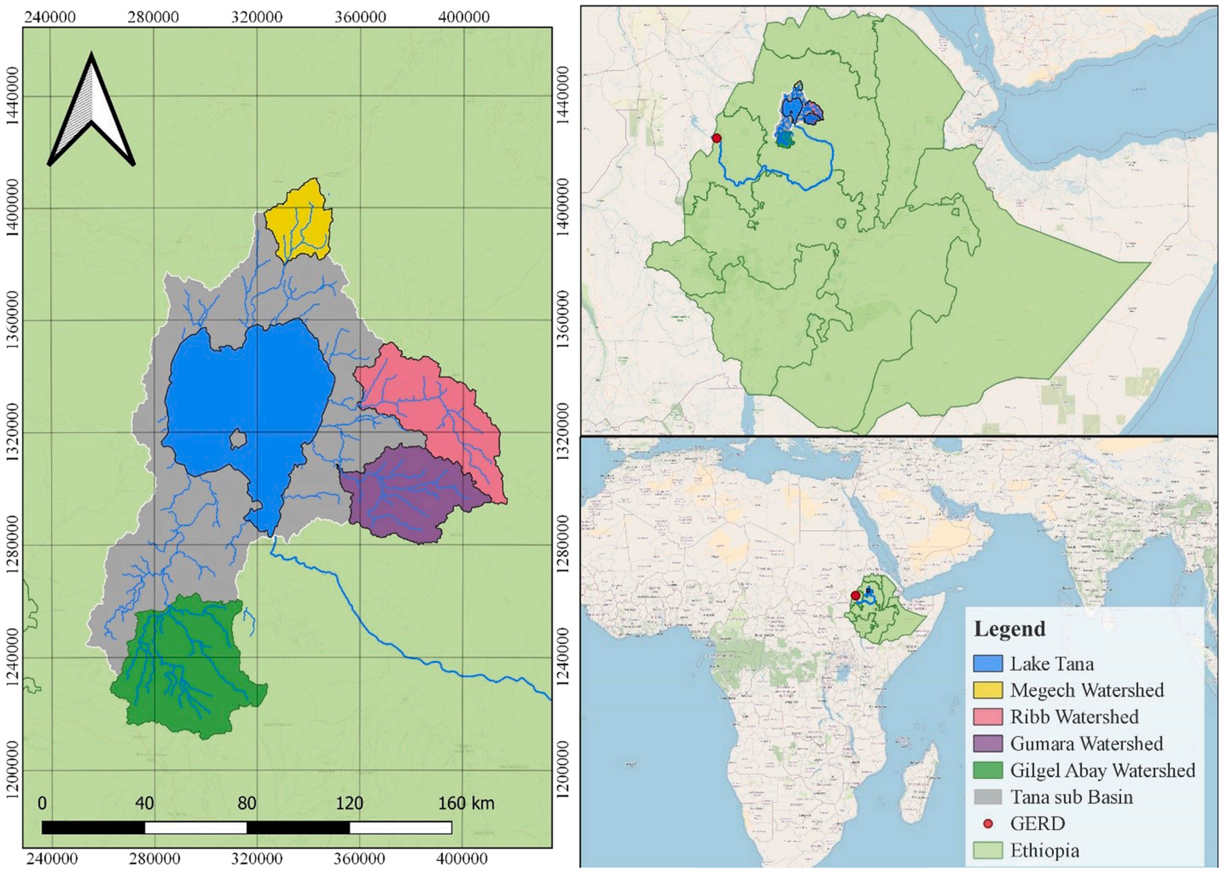

Fig. 1. Study area location map.

Mengistu et al., 2021; Roth et al., 2018). Numerous studies indicate that the hydrology of headwater catchments of the upper Blue Nile basin in Ethiopia has been influenced by climate change (Kim and Kaluarachchi, 2009; Malede et al., 2022; Worqlul et al., 2018). Whereas there are many climate change studies conducted in the Lake Tana basin, very few studies used the RCP scenarios. For instance, the study conducted by (Chakilu et al., 2020; Tigabu et al., 2021) used the RCP 8.5 scenario, but the studies were conducted only on one or two catchments within the basin, which limits our understanding of the potential impacts of climate change in the entire basin. Besides, most of the previous studies conducted in the basin focused on projecting future climate under Special Report on Emissions Scenarios (SRES). For example, Setegn et al. (2011) used the A2 scenario, while Adem et al. (2014) used A2 and B2 emission scenarios with a single climate model.

This study focused on how much the highest emission scenario (RCP8.5), suggested by the Fifth IPCC Assessment Report (AR_5) (IPCC, 2014), influences the stream flow nature of the four gauged watersheds of Lake Tana Basin, which contributes more than 60% of the total flow of the Nile River (Mulat and Moges, 2014) by using six Global Climate Models (GCM) in (2071–2100) with relative to (1971–2000). Due to the inadequate number of meteorological stations in the basin, and considering that most of the existing stations do not have long-term historical recorded data for regional downscaling, Global Climate Models (GCM) were directly used through correcting the biases using CMhyd software. The finding of this study gives important indications on the extent to which this highly demanded water resources for both upper and lower catchment communities, will be affected by climate change, and it also gives essential output for policymakers concerned about the reduction of climate change vulnerability of water resources in the planning process of different micro and macro projects, including the Grand Ethiopian Renaissance Dam (GERD).

2. Material and methods

2.1. Study area description

Lake Tana basin is located in the North-Western Highlands and stretches between 10.95° and 12.78°N latitudes and 36.89° and 38.25°E longitudes with a drainage area of about 15,096 km^2 of which, 3063 km^2 of land is covered with Lake Tana (Fig. 1). Lake Tana is the largest lake in Ethiopia, covering a surface area of 3000–3600 km^2 at an elevation of 1800 m above sea level and a maximum depth of 15 m. The climate of the Lake Tana sub-basin is dominated by tropical highland monsoon with most of its rainfall occurring between June and September. More than 93% of the flow of the lake is collected from four major rivers which are Gilgel Abay, Gumara, Ribb, and Megech (Setegn, 2010). Gilgel Abay is the largest watershed in the Lake Tana sub-basin which covers 1754 km^2; followed by Ribb, Gumara, and Megech watersheds which cover 1407 km^2, 1272 km^2, and 514 km^2, respectively. According to (Conway and Schipper, 2011), most of the rainfall (70–90% total rainfall) in the region occurs from June to September, and the mean annual precipitation of the study area ranges from 1200 to 1600 mm based on data from 1961 to 2000. The temperature of the basin varies between 9 °C and 28 °C.

Based on the FAO soil classification map of the world (FAO and UNESCO, 1977), Chromic Luvisols, Eutric Cambisols, Eutric Fluvisols, Eutric Leptosols, Eutric Regosols, Eutric Vertisols, Haplic Alisols, Haplic Luvisols, Haplic Nitisols and Lithic Leptosols are the

Table 1
Meteorological stations with their accessed data and purposes used in the study.

Stations	Latitude	Longitude	Accessed data		Data used for:
			Temperature	Rainfall	
Gondar	12.3	37.25	1952–2009	1952–2009	Bias correction, SWAT model calibration & validation, and projection of future climate for simulation of future stream flow
Makisegnit	12.39	37.55	1996–2008	1987–2008	SWAT model calibration & validation, and projection of future climate for Simulation of future stream flow
Addis Zemen	12.12	37.77	1996–2009	1997–2009	SWAT model calibration & validation, and projection of future climate for simulation of future stream flow
Debretabor	11.86	37.99	1951–2009	1951–2009	Bias correction, SWAT model calibration & validation, and projection of future climate for simulation of future stream flow
Werota	11.92	37.69	1992–2008	1969–2007	SWAT model calibration & validation, and projection of future climate for simulation of future stream flow
Wanzaye	11.78	37.67	2000–2009	1984–2008	SWAT model calibration and projection of future climate for simulation of future stream flow
Bahir Dar	11.60	37.36	1961–2009	1961–2009	Bias correction, SWAT model calibration & validation, and projection of future climate for simulation of future stream flow
Dangila	12.25	36.84	1954–2009	1954–2009	Bias correction, SWAT model calibration & validation, and projection of future climate for simulation of future stream flow
Injibara	10.99	36.92	1984–2008	1954–2008	SWAT model calibration & validation, and projection of future climate for simulation of future stream flow
Adet	11.27	37.49	1989–2009	1989–2009	SWAT model calibration & validation, and projection of future climate for simulation of future stream flow
Sekela	10.98	37.21	1989–2008	1988–2008	SWAT model calibration & validation, and projection of future climate for simulation of future stream flow
Wetet Abay	11.37	37.04	1987–2008	1987–2008	SWAT model calibration & validation, and projection of future climate for simulation of future stream flow

major soil types in the basin. The majority of the land area, 51.3%, of the Lake Tana Basin is used for agriculture, 29% is an agro-pastoral area, and 20% of the basin is covered by the lake water (Setegn et al., 2008).

2.2. Climate and hydrological data collection and processing

Meteorological data were obtained from the National Meteorological Agency of Ethiopia. Some of the data which span 30 years (1971–2000) were used for bias correction of climate model outputs. Twelve meteorological stations were used in and near the study area. Although there are more numbers of meteorological stations in the study area, many of them do not have adequate data and are full of missing values even in recorded data. The missing values were replaced by the long-term average recorded values of the corresponding dates of the preceding years and the years after the missed one to compare and evaluate the deviation of the data produced from climate models. During the SWAT model calibration and validation process, the missing data were replaced by − 99 which is compatible with the SWAT model. Table 1.

Climate model data were obtained from the Earth System Grid Federation (ESGF) website (https://esgf-node.llnl.gov/projects/esgf-llnl/), which is hosted by the United States of America, Department of Energy, Lawrence Livermore National Laboratory. Given that most of the meteorological stations in the Lake Tana basin do not have long-term historical recorded data for regional downscaling, Global Climate Models (GCM) were directly used through bias correction using CMhyd software. Precipitation and temperature data are projected by six Global Climate Models including CanESM2, EC-EARTH, CNRM-CM5, HadGEM2-ES, NORESM1-M, and CSIRO-Mk3–6–0 in Coupled Model Inter-comparison Project Phase 5 (CMIP5). The data are produced under the experiment of the Representative Concentration Pathway (RCP8.5) emission scenario.

Flow data of the four watersheds (Gilgel Abay, Gumara, Ribb, and Megech) were collected from the Ministry of Water and Energy of Ethiopia for calibration and validation of the SWAT model. Like meteorological data, flow data were also collected on a daily time scale with missing values replaced by − 99.

2.3. Geophysical data collection and processing

Besides climatic data, geophysical data such as land use/cover, soil, and altitude (DEM) were required to run the hydrological model (SWAT). The land use/cover data were obtained from the Ministry of Water and Energy of Ethiopia. Soil data of the study area were also obtained from the Digital Soil Map of the World website (https://data.apps.fao.org/map/catalog/srv/eng/catalog.search#/metadata/446ed430–8383–11db-b9b2–000d939bc5d8), which is digitized by FAO-UNESCO Soil Map of the World with 1:5000000 scale. SRTM Digital Elevation Model (DEM) data with 30 m * 30 m resolution was collected from the United State Geological Survey (USGS) website (https://earthexplorer.usgs.gov/). The altitude data was used for watershed delineation and slope classification in Hydrological Response Unit (HRU) definition and analysis process.

2.4. Bias correction of climate models data

Climate data are obtained from global-scale climate models. Climate variables such as rainfall and temperature obtained from such coarse resolution climate models are highly influenced by local topographies like mountains which may not probably be taken into consideration in the global climate models development process because of their coarse resolution. Thus, to minimize the deviation of climate models output from the real observed data of meteorological stations, the bias correction process was needed and it was done using variance scaling and power transformation methods for temperature and precipitation, respectively using CMhyd software (Rathjens et al., 2016). The reason why these two methods were selected for this study was, that both are more efficient than other methods in frequency-based statistics in other studies (Fang et al., 2015; Teutschbein and Seibert, 2012). Precipitation data obtained from all climate models were corrected by fitting them to the thirty years (1971–2000) data and measured for their Coefficient of Variation (CV) in the power transformation process. In this nonlinear correction, each daily precipitation amount P is transformed into a corrected P * by using Eq. (1) as follows:

$$P^{*} = aP^{b} \tag{1}$$

The coefficient “a” and the superscript “b” were determined iteratively. The mean value of “b” was determined by equating the CV of the observed value of precipitation with that simulated value on a monthly basis, and the coefficient” a” was determined by equating the mean value of observed precipitation with that simulated value for the comparison period.

Bias correction for temperature only involved scaling and shifting to adjust the mean and variance of simulated and observed climate data (Terink et al., 2010; Ho et al., 2012) by fitting it to thirty years period (1971–2000) data and the standard year’s deviation (SD). Thus the corrected daily temperature (T_{corr}) was obtained by using the following Eq. (2):

$$T_{corr} = \overline{T}_{obs} + \frac{\sigma(T_{obs})}{\sigma(T_{gcm})}\left(T_{gcm} - \overline{T}_{gcm}\right) \tag{2}$$

Where T_{corr} is the corrected daily temperature; T_{gcm} is the uncorrected daily temperature obtained from the climate model; T_{obs} is the observed daily temperature; an overbar (“¯”) denotes the mean value of the variable and σ is the standard deviation.

2.5. SWAT model setup and simulation

Soil Water Assessment Tool (SWAT) is a semi-distributed small watershed or large river basin scale hydrological model, which simulates the quality, quantity of surface, and groundwater. It also simulates sediment transport on a particular watershed while predicting the environmental impacts of land use, land management practices, and climate change. It is widely used in the assessment of soil and water conservation and non-point pollution control in river basins (Neitsch et al., 2002).

The model requires daily climate data and geophysical data to simulate surface runoff, groundwater flow, and evapotranspiration of watersheds. The model starts from the watershed characterization process, and basically, it passes six important steps: (1) watershed delineation, (2) Hydrological Response Unit (HRU) definition and analysis, (3) climate and weather data formation, (4) Simulation, (5) model calibration, and (6) model validation.

SRTM DEM data of the entire Lake Tana basin was used for river networking and watershed delineation through the "burn-in" method. In the process, four outlets were selected for the study area, and each watershed was delineated with a combination of sub-watersheds. Sub-watersheds were further classified into Hydrological Response Units (HRUs) using land use, soil, and slope distribution process. All land use, soil, and slope classes in each sub-basin were considered in the HRU definition process. Surface runoff is estimated separately for each sub-basin and routed to quantify the total surface runoff of the basin using the following equation (Eq. (3)) (Neitsch et al., 2002).

$$SW_t = SW_0 + \sum_{i=1}^{t} \left(R_{day} - Q_{surf} - E_a - W_{sweep} - Q_{gw}\right)_i \tag{3}$$

Where SW_t is the final soil water content (mm), SW_o is the initial soil water content on the day i (mm), t is time (days), R_{day} is the amount of precipitation on the day i (mm), Q_{surf} is the amount of surface runoff on the day i (mm), E_a is the amount of evapotranspiration on the day i (mm), W_{seep} is the amount of water entering the vadose zone from the soil profile on the day i, and Q_{gw} is the amount of groundwater flow on the day i (mm). The amount of surface runoff is calculated using the following formula (Eq. (4)).

$$Q_{surf} = \frac{\left(R_{day} - I_a\right)^2}{\left(R_{day} - I_a + S\right)} \tag{4}$$

Where Q_{surf} is the accumulated runoff or rainfall excess (mm); R_{day} is the height of rainfall for the day (mm); Ia is the initial abstractions (canopy interception, surface storage, infiltration before runoff) (mm), and S is the retention parameter. Therefore, retention parameter S is defined as Eq. (5):

$$S = 25.4\left(\frac{1000}{CN} - 10\right) \tag{5}$$

Where CN is the curve number for the day and the initial abstractions, Ia, are commonly approximated as 0.2 S. Eq. (6) is represented as follows:

$$Q_{surf} = \frac{\left(R_{day} - 0.2S\right)^2}{\left(R_{day} + 0.8S\right)} \tag{6}$$

The runoff will only occur when $R_{day} > I_a$.

2.6. SWAT model calibration and validation

Once the flow was simulated with default parameters, sensitive parameters were selected using the sensitivity analysis process. For the four watersheds, ten and seven years of climate data were used for calibration and validation, respectively. These years were selected based on the availability of data. Based on the sensitivity analysis result, eleven parameters that have a prominent influence on

Table 2
SWAT model parameters with their description and ranges of values.

N_o.	Parameters	Description	Maximum value	Minimum value
1	R_CN2.mgt	Initial SCS CN II value	0	1
2	V_ALPHA_BF.gw	Baseflow alpha-factor (days)	-25	25
3	V_ESCO.hru	Soil evaporation compensation factor	0	1
4	V_GW_DELAY.gw	Groundwater delay (days)	0	10
5	V_GW_REVAP.gw	Groundwater "revap" coefficient (days)	0.02	0.2
6	A_SLSUBBSN	Average slope length (m)	-0.5	1
7	A_SOL_AWC	Available water capacity (mm water/mm soil)	0	1
8	A_SOL_K	Saturated hydraulic conductivity (mm/hr)	-0.5	1
9	A_SOL_Z	Soil depth (mm)	-25	25
10	V_SURLAG	Surface runoff lag time (days)	0	12
11	V_GWQMN	Threshold water depth in the shallow aquifer for flow (mm)	0	10

the streamflow of watersheds were selected (Table 2), and the value of each parameter in the four watersheds was determined by the calibration process. The calibration process was done by using SWAT-CUP (SWAT-Calibration and Uncertainty Programs) version 12 software and the Sequential Uncertainty Fitting (SUFI-2) algorithm. The fitted value of parameters was observed by iterating 2000 simulations through automatically adjusting the values based on the range of adjustment domain. The output produced by using selected parameters and their adjusted values were compared with the observed streamflow of the watersheds so that the efficiency of the SWAT model was evaluated. The efficiency of the model was evaluated using statistical variables that determine the fitness of simulated flow with the measured flow data of watersheds. Those statistical variables are Nash–Sutcliffe Efficiency (NSE), and Relative Volume Error (RVE), shown in Eqs. (7) and (8), respectively.

$$NSE = 1 - \frac{\sum_{i=1}^{n}\left(Q_{sim(i)} - Q_{obs(i)}\right)^2}{\sum_{i=1}^{n}\left(Q_{sim(i)} - \overline{Q}_{obs}\right)^2} \tag{7}$$

Where Q_{obs} and Q_{sim} represent the observed and simulated daily stream flows at the i^{th} time steps respectively, n refers to the number of days in the simulated or observed time series period. The overbar (¯) symbol represents the mean value which indicates the average value of streamflow. The value of Nash–Sutcliffe Efficiency (NSE) ranges between 1 and $-\infty$; 1 shows the best fit of the model or that the model simulates similar values of streamflow with the observed values. A value between 0 and 1 is considered an acceptable level of performance (Nash and Sutcliffe, 1970).

$$RVE = \frac{\sum_{i=1}^{n}\left(Q_{obs(i)} - Q_{sim(i)}\right)}{\sum_{i=1}^{n} Q_{obs(i)}} * 100\% \tag{8}$$

RVE indicates the ratios of the sum of differences in the observed and simulated value of streamflow to the total observed streamflow. The optimal value of RVE is 0. A positive value indicates underestimation and a negative value indicates overestimation (Gupta et al., 1999).

3. Result and discussion

3.1. *The efficiency of climate models*

In this study, six climate models were used to predict future climate in the study area. The efficiency of each model was evaluated by comparing their historical data with station observed data. The error in rainfall and temperature are analyzed on monthly basis. The model error of rainfall ranges from an absolute value of 0.05–1.94%. The maximum variation is observed in August by the NORESM1-M climate model, and the minimum is observed in January by the CSIRO-Mk3–6–0 climate model. Almost all climate models reasonably capture the station-measured rainfall, especially in the winter season (December–March) (Fig. 2). Indeed, the change is more prominent in the summer season because rain is not common in the winter seasons in the study area. In general, the rainfall data produced by climate models are consistent with the measured data on the stations.

All climate models except CNRM-CM5 overestimated the maximum temperature in six consecutive months (from December to

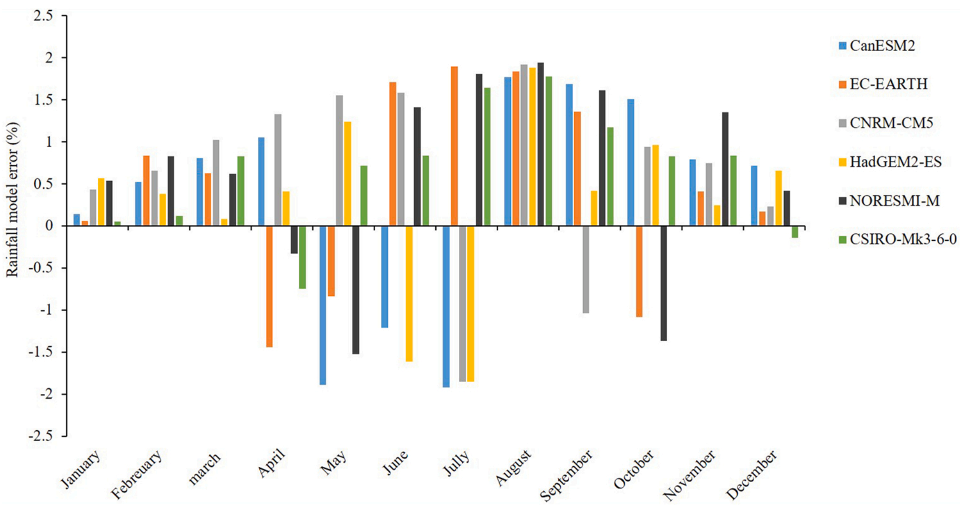

Fig. 2. Rainfall model error.

May). The error ranges from the absolute value of 0.01 °C which is predicted in September CSIRO-Mk3–6–0 and January by HadGEM2-ES to 0.5 °C predicted in March by the CNRM-CM5 climate model. The overall deviation of the model in maximum temperature is 0.19 °C, 0.03 °C, 0.25 °C, 0.14 °C, 0.12 °C, and 0.16 °C in CanESM2, EC-EARTH, CNRM-CM5, HadGEM2-ES, NORESM1-M, and CSIRO-Mk3–6–0 climate models, respectively (Fig. 3).

All climate models are relatively more efficient in minimum temperature than the maximum temperature in capturing the measured data. The errors of models range from 0.01 °C to 0.35 °C, and the maximum error was recorded in October by the CNRM-CM5 climate model. Unlike maximum temperature, some climate models underestimate the minimum temperature on monthly basis. Generally, on average, errors by CanESM2, EC-EARTH, CNRM-CM5, HadGEM2-ES, NORESM1-M, and CSIRO-Mk3–6–0 are 0.03 °C, 0.04 °C, 0.07 °C, 0.09 °C, 0.02 °C, and 0.05 °C, respectively (Fig. 4).

3.2. Change in rainfall

In the last thirty years of this century, rainfall is predicted to increase in the summer and autumn seasons in all climate models except the CNRM-CM5 model which predicted an increase in rainfall in September, and NORESMI-M in October. Seasonally, the change in rainfall ranges from the absolute value of 0.83–29.75% (Fig. 5). The maximum change is forecasted by the CNRM-CM5 climate model in November. Most of the climate models predicted that rainfall will decrease in the spring/pre-summer season. The maximum decreasing change is observed in March which is − 9.26% by the CanESM2 climate model. As far as the region has been getting rainfall in the summer season (Conway and Schipper, 2011), it is obvious that the change is not that much expected to be high in the winter season and this study showed the same result. On an annual average basis, the change is relatively lower than the change in the monthly time step. Annually, the change ranged from 2.45% to 7.17%, in which the maximum change was predicted by CSIRO-Mk3–6–0. In general, the annual mean rainfall is expected to change by 6.85%, 2.45%, 4.89%, 2.46%, 2.57%, and 7.17% under CanESM2, EC-EARTH, CNRM-CM5, HadGEM2-ES, NORESM1-M, CSIRO-Mk3–6–0 climate models, respectively within one hundred years (Fig. 8).

3.3. Change in temperature

SWAT model requires daily maximum and minimum air temperature which may be read from records of observed data or may be generated (Neitsch et al., 2002). Seasonally, the maximum temperature is expected to increase with a range of 2.93 °C and 5.17 °C under all climate models based on the RCP 8.5 climate change scenario in the last thirty years of the 21st century. The lowest change in maximum temperature was forecasted by the CNRM-CM5 climate model in November, whereas the highest change is forecasted by CSIRO-Mk3–6–0 in March (Fig. 6). The change is higher in the winter than the summer season in almost all climate models. On an average basis, the highest change was observed in March which is 4.61 °C, and the lowest is 3.48 °C in November (Fig. 6). Temperature is one of the most important parameters for estimating the evapotranspiration which can potentially reduce the water availability in the catchments in the SWAT model (Neitsch et al., 2002). Because the area is dry in the winter season, and potential evapotranspiration which is used for water balance computation in this study is considering that the availability of moisture in the soil is sufficient enough (Allen et al., 1998), this highest change in maximum temperature observed in March may not have a significant effect in actual evapotranspiration of the catchments. Annually, the maximum temperature is expected to increase by 4.12 °C, 4.05 °C, 4.03 °C,

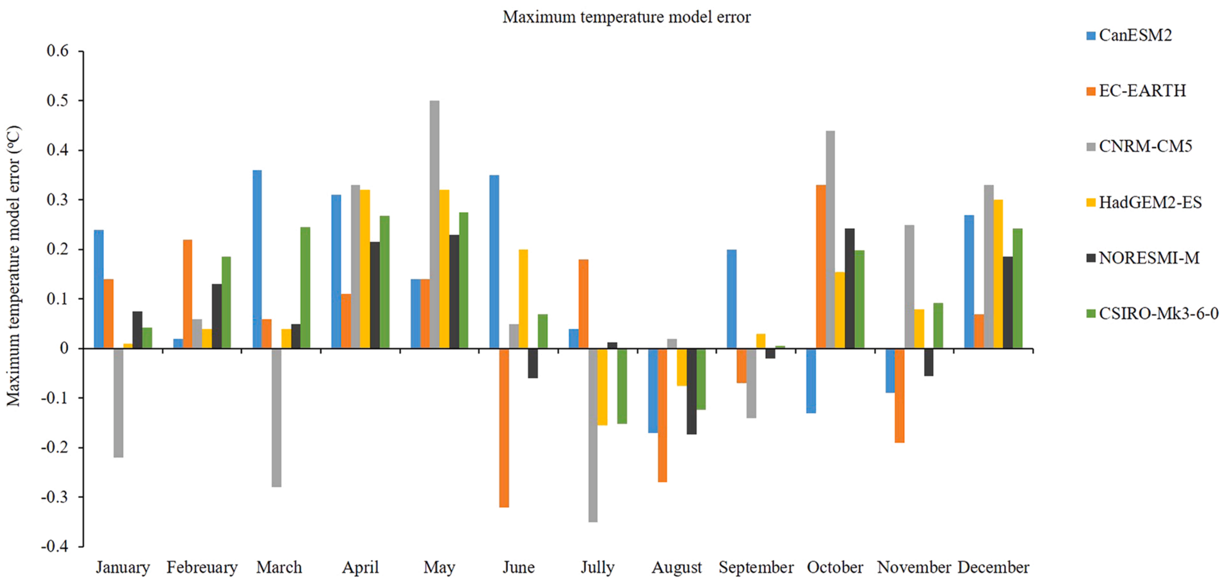

Fig. 3. Maximum temperature model error.

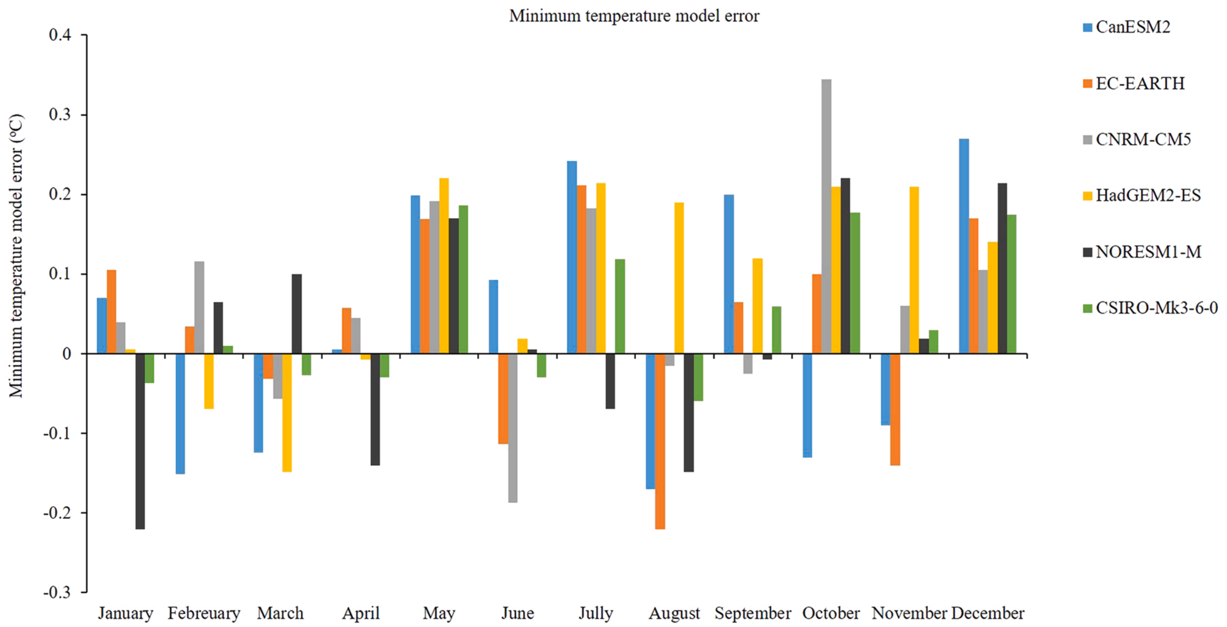

Fig. 4. Minimum temperature model error.

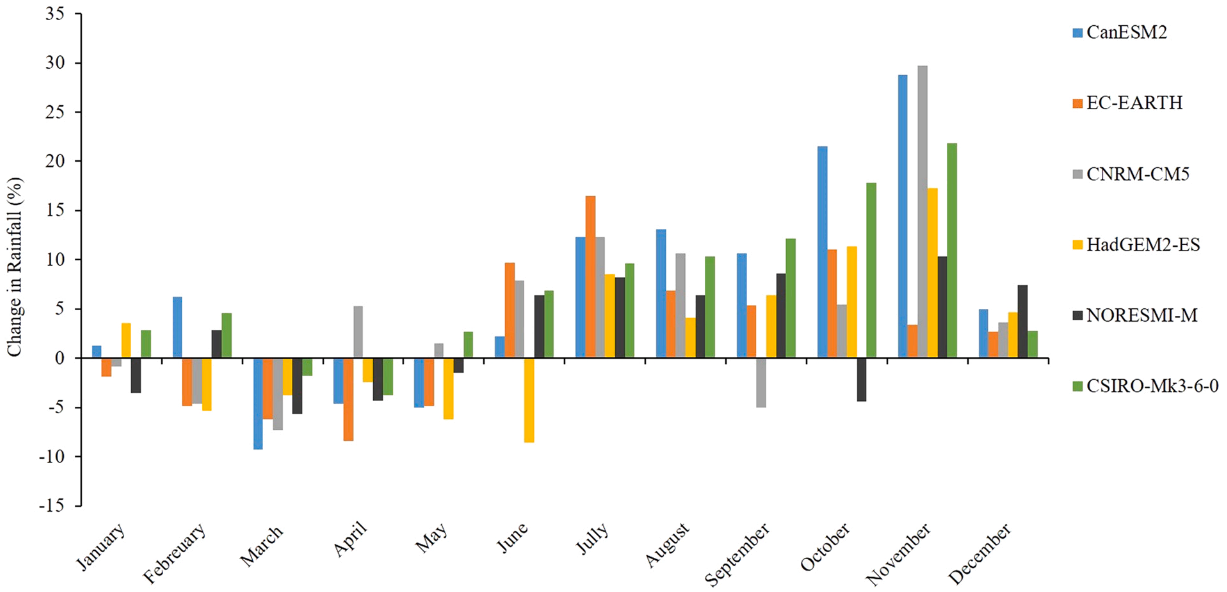

Fig. 5. Change in precipitation in Lake Tana basin.

3.99 °C, 3.96 °C, and 3.89 °C, under CSIRO-Mk3–6–0, HadGEM2-ES, CanESM2, CNRM-CM5, NORESMI-M, and EC-EARTH climate models respectively (Fig. 8).

The overall change in minimum temperature follows a more or less similar seasonal pattern to the change in maximum temperature except for the difference in time when the highest changes are observed. The average change in minimum temperature ranges from 3.08 °C observed in October by EC-EARTH to 4.79 °C observed in April by the CNRM-CM5 climate model (Fig. 7). Like maximum temperature, the change in minimum temperature is also higher in the winter season. In terms of average values of changes in all climate models, the highest change in minimum temperature is expected to be 4.42 °C in April. On annual basis, the change in minimum temperature is not showing significant variation between the climate models we used. At the end of thirty years of this century, the mean minimum temperature is expected to increase by 4.11 °C, 4.06 °C, 4.04 °C, 4.00 °C, 3.88 °C, 3.86 °C under CSIRO-Mk3–6–0, CanESM2, HadGEM2-ES, CNRM-CM5, EC-EARTH, and NORESM1-M climate models, respectively (Fig. 8).

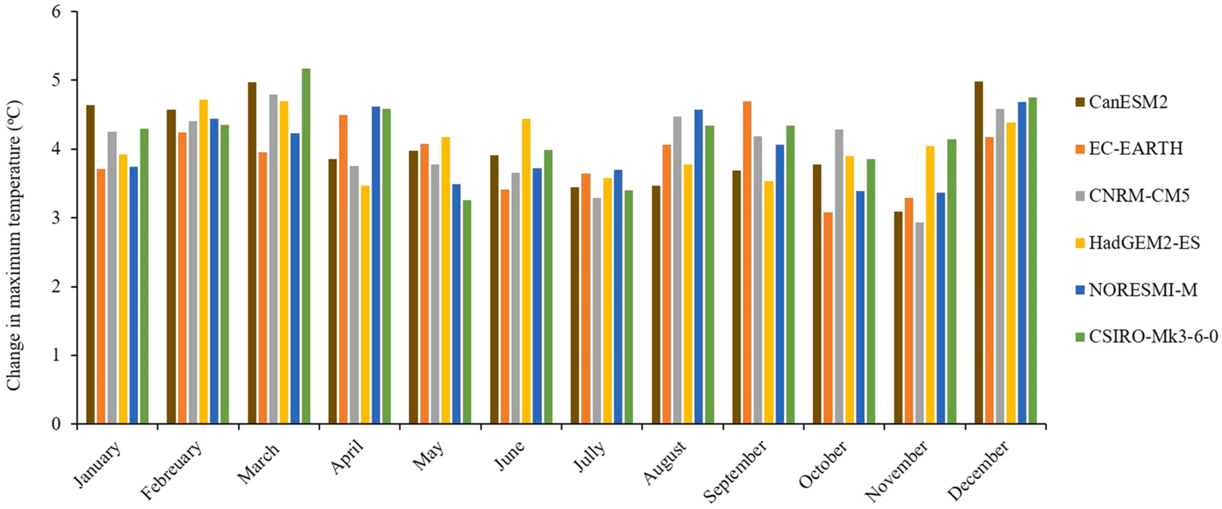

Fig. 6. Change in maximum temperature in Lake Tana basin.

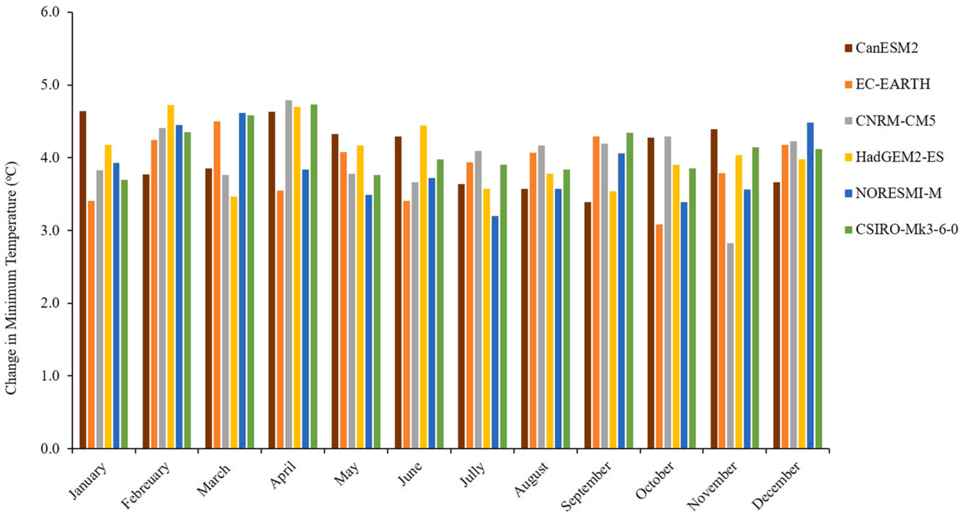

Fig. 7. Change in minimum temperature in Lake Tana basin.

3.4. SWAT model efficiency

SWAT model has a good efficiency in the gaged watersheds of the Lake Tana basin. The default efficiency of the model was very poor in both statistical parameters which are Nash–Sutcliffe Efficiency (NSE), and Relative Volume Error (RVE). Comparatively, the highest efficiency in terms of NSE was observed in the Gumara watershed (0.18), but in terms of RVE, it was good in the Ribb watershed (28.69%) in default simulation. The worst efficiency of the model was observed in the Megech watershed in terms of both NSE and RVE, the values were − 0.32 and − 48.52, respectively (Table 4).

To enhance the efficiency of the SWAT model, some additional parameters were included and a total of 11 important parameters were selected after sensitivity analysis was done, and the values of the parameters were calibrated using automatic calibration and manual calibration processes. In the sensitivity analysis process, the parameter which has the highest value of the absolute value of t-stat and the lowest value of the P-value is taken as the most sensitive parameter (Neitsch et al., 2002). Among 11 parameters five of the most sensitive parameters in each watershed with their fitted values are presented in (Table 3).

The model was more efficient in the Gilgel Abay watershed in both calibration and validation process in terms of NSE (0.86). Even though it shows some improvement through calibration, the model was still weak in the Megech watershed, and statistically, the efficiency of the model (NSE) in the watershed was 0.51, and 0.54 in the calibration and validation process, respectively. The RVE in this watershed recorded negative − 8.84%, and − 6.62% in the calibration and validation process, respectively. These negative RVE values indicate that the model overestimated the simulated streamflow relative to the measured value (Table 4).

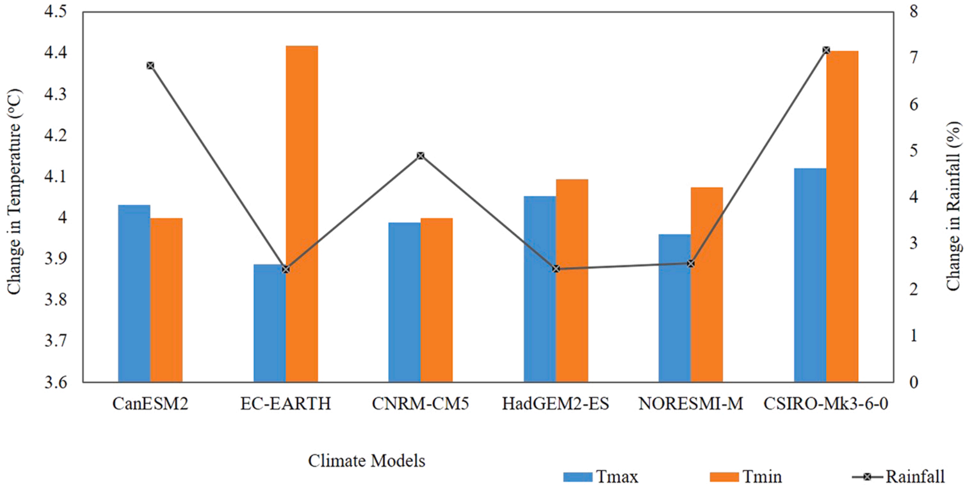

Fig. 8. Change in mean annual Tmax, Tmin, and precipitation.

Table 3
The most five model parameters sensitivity, ranges of values, and fitted values in SWAT model.

Watershed	Parameter	t-stat	P-value	Fitted value	Rank
Gumara	R_CN2.mgt	-10.14	0	0.14	1
	V_ALPHA_BF.gw	5.48	0	-12	2
	V_ESCO.hru	-3.07	0.03	0.42	3
	V_GW_DELAY.gw	-2.9	0.09	7.34	4
	V_GW_REVAP.gw	-2.23	0.11	0.19	5
Gilgel Abay	R_CN2.mgt	-58	0	-0.18	1
	V_ALPHA_BF.gw	10.8	0	0.12	2
	A_SOL_K.sol	6.1	0	0.47	3
	V_GW_REVAP.gw	-1.2	0.2	0.10	4
	V_GWQMN.gw	1	0.3	1.31	5
Ribb	V_ESCO.hru	3.76	0.01	0.5	1
	R_SOL_AWC.sol	3.55	0.01	0.9	2
	V_EPCO.hru	2.55	0.04	0.7	3
	R_CN2.mgt	-1.95	0.09	2.37	4
	V_ALPHA_BF.gw	1.77	0.12	0.5	5
Megech	R_CN2.mgt	-10.55	0.00	-0.02	1
	V_ALPHA_BF.gw	-8.27	0.00	0.76	2
	V_GW_DELAY.gw	− 2.70	0.01	5.37	3
	V_GWQMN.gw	2.26	0.03	0.55	4
	A_SOL_K.sol	1.90	0.06	-0.17	5

Table 4
SWAT model efficiency in the four watersheds.

Watersheds	Default efficiency		Calibration		Validation	
	NSE	RVE (%)	NS	RVE (%)	NSE	RVE (%)
Gilgel Abay	0.15	32.41	0.86	1.31	0.84	1.36
Gumara	0.18	36.84	0.67	1.25	0.63	1.88
Ribb	0.09	28.69	0.71	1.14	0.74	1.07
Megech	-0.32	-48.52	0.51	-8.84	0.54	-6.62

The calibrated values of parameters were also verified by independent climate data, and it shows consistent efficiency with the calibrated one. As it is shown in (Fig. 9), the model captured the peak flows in some years; whereas it overestimated and underestimated in some other years in all watersheds. As it can be shown on the graph (Fig. 9), in the Megech watershed, simulated flow is higher than the observed flow in both calibration and validation time. In this simulation process, the model does not consider irrigation and other small scale water work projects that can reduce the stream flow at the lower catchment of the watershed. On the upper part of the Megech watershed, there is one dam (Angereb dam) which is used for the domestic water supply of Gondar town (Haregeweyn et al., 2012). Because, the dam stores water during the rainy season, the peak simulated flow is higher than the observed flow as it can be shown in (Fig. 9).

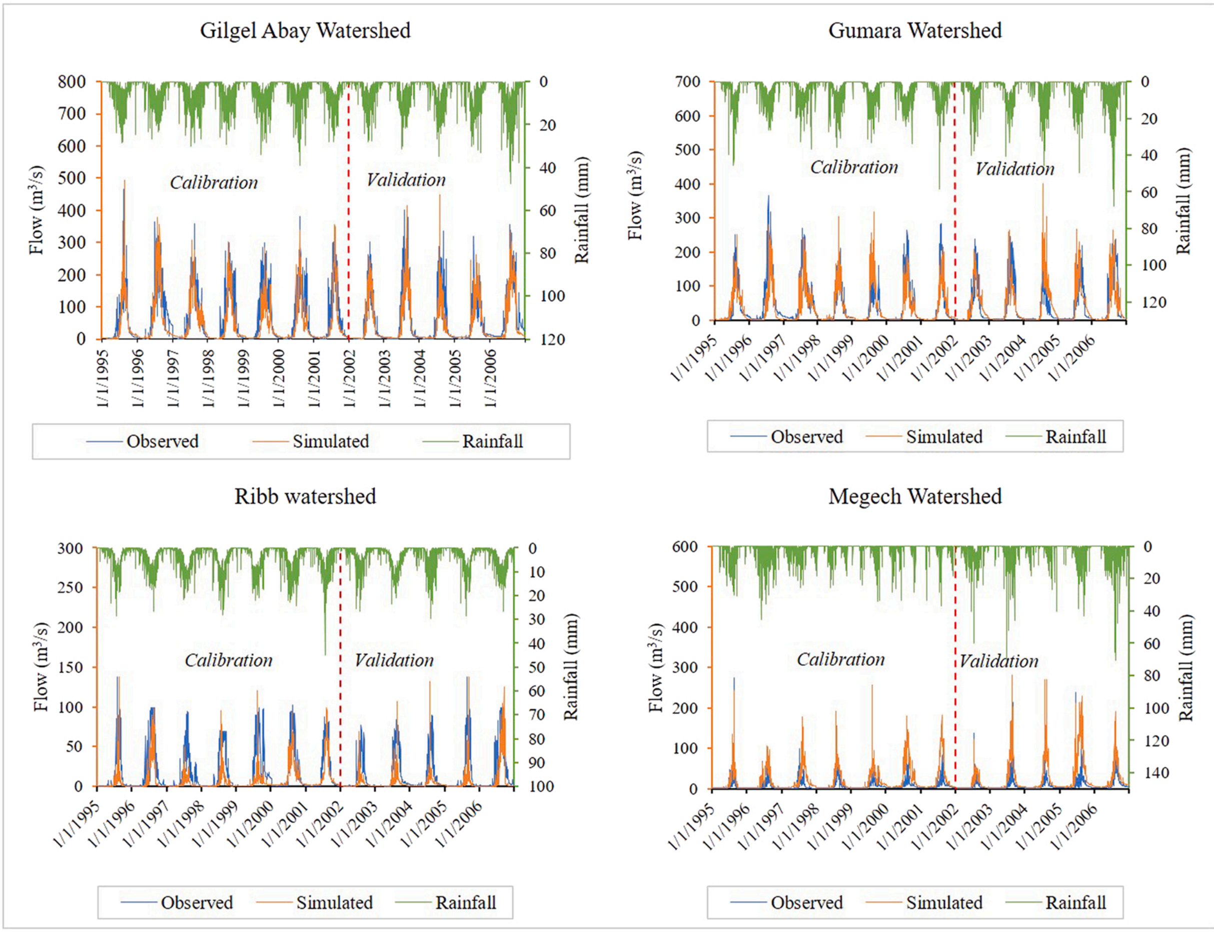

Fig. 9. Simulated flow Vs Observed flow of watersheds.

3.5. *Impacts of climate change on streamflow*

The streamflow in the four major watersheds of Lake Tana sub-basin under the worst Representative Concentration Pathway (RCP 8.5) scenario shows visible changes in the last thirty years of this century. In all watersheds, seasonally, the change is more prominent in summer and the beginning of autumn. The impact of climate change on the dry season flow of the four watersheds is much less than the impact observed in rainy seasons. According to (Chakilu and Moges, 2017; Gebrehiwot et al., 2010; Mekonnen et al., 2018; Rientjes et al., 2011) studies conducted in the region, and (Shao et al., 2018; Yihdego and Webb, 2013) out of the region, the dry season flow of watersheds is affected by the land-use change of the catchments. Even though the study area commonly gets rainfall in the summer season, especially in July and August, the change in rainfall was higher in the following three months. In all watersheds, the maximum value of change in streamflow was observed in November (Figs. 10–13). Unlike in the Ribb watershed, in the other three watersheds, the maximum change is shown under the CanESM2 climate model prediction. Given that the four watersheds are close to each other, the minimum, maximum, and average change of streamflow in all climate models did not show a significant variation among the watersheds. The maximum change in all watersheds ranges from 25% to 28% (approximately) in all climate models. The maximum value of changes in Gilgel Abay, Gumara, Ribb, and Megech is 27.47%, 26.47%, 27.82%, and 24.97%, respectively. Even though the change in streamflow between watersheds is not showing considerable variation, the change between the six climate models within each watershed showed great variation.

In the Gilgel Abay watershed, the change ranges from 0.52% in June by the NORESM1-M climate model to 27.47% in November by CanESM2 including the decreasing change. The change under almost all climate models except under CNRM-CM5 in April shows a decreasing value in the winter and spring season and it ranges from − 0.59% to − 5.95% (Fig. 10).

Like the Gilgel Abay watershed, in the Gumara watershed, the maximum change in streamflow is shown in November, and it is produced because of the CanESM2 climate model. The change in this watershed, except HadGEM2-ES in June, and NORESM1-M in October, under all climate models in all months of summer and autumn seasons, showed an increasing trend. In the Gumara watershed, the change ranges from − 0.71% (decreasing) in January under the CNRM-CM5 climate model to 26.47% in November under the CanESM2 climate model (Fig. 11). The result is consistent with other studies with different climate models (Ayele et al., 2016), and

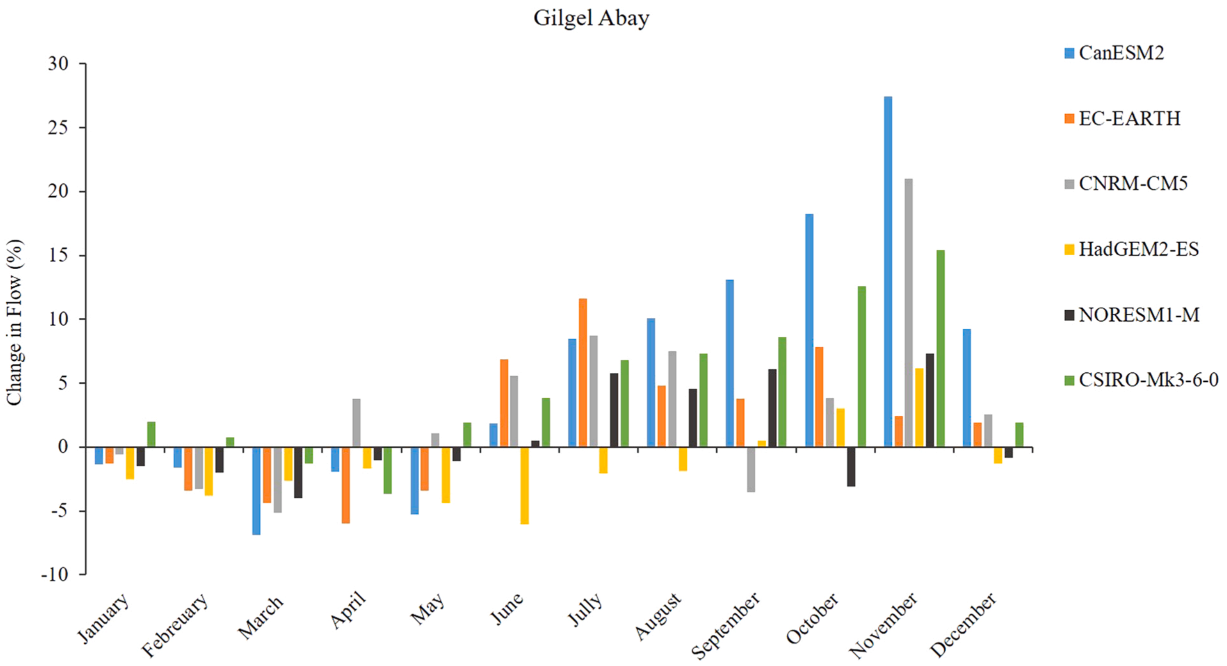

Fig. 10. Change in streamflow in Gilgel Abay watershed.

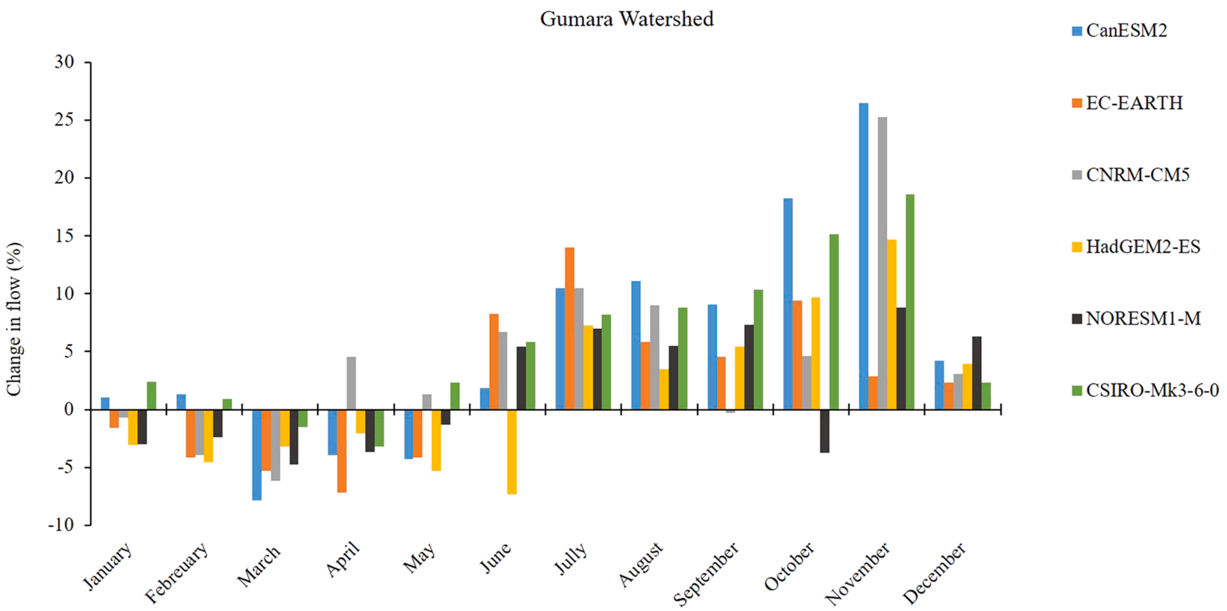

Fig. 11. Change in streamflow in Gumara watershed.

different hydrological models (Haile et al., 2017). This watershed is one of the highly vulnerable areas of the Lake Tana basin to climate change due to much of the upper catchment of the watershed being covered by mountainous land and being used for intensive agricultural activities (Chakilu and Moges, 2017). During the summer season, the area gets a high amount of rainfall which can result in flooding in the lower catchment of the watershed, and in another way, it is also highly exposed to hydrological drought in the winter (dry) season because of the expansion of agriculture, and plowing of sloppy areas without applying any soil and water conservation mechanisms (Mena, 2018) which enable the water to infiltrate into the soil and join the groundwater to enhance the base flow of the river (Dams et al., 2008; Zhang and Schilling, 2006).

Unlike the other three watersheds, in the Ribb watershed, the maximum change in streamflow was observed under CNRM-CM5, but similar to others, it is observed in November (Fig. 12). Though there are some variations in the values of change in streamflow under all

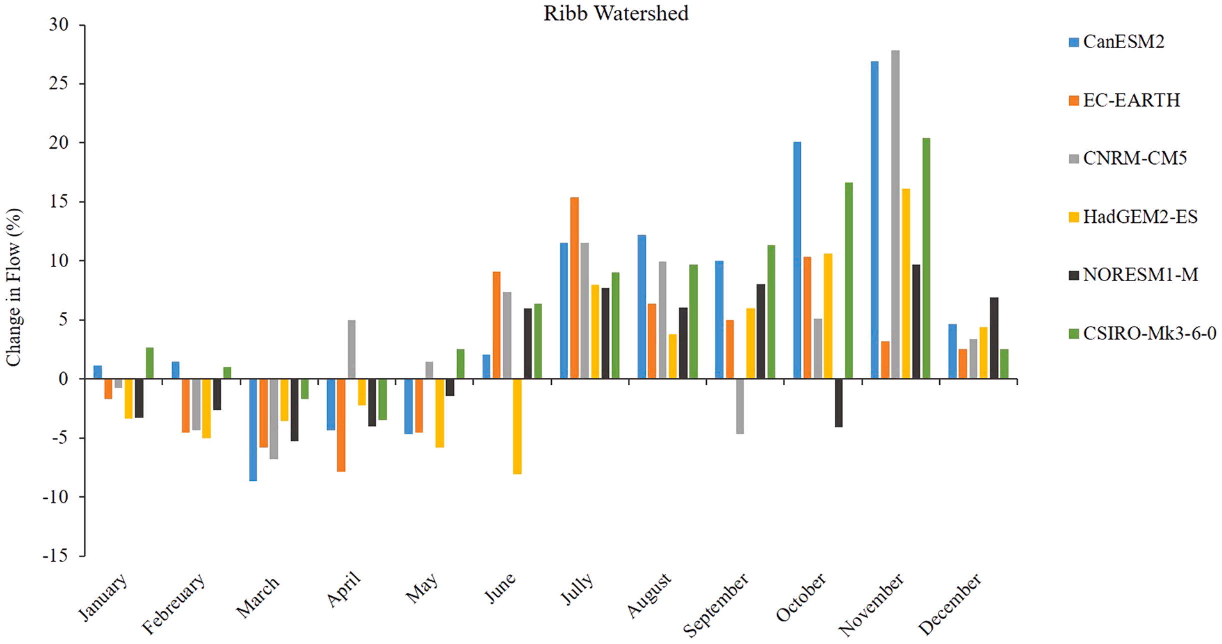

Fig. 12. Change in streamflow in Ribb watershed.

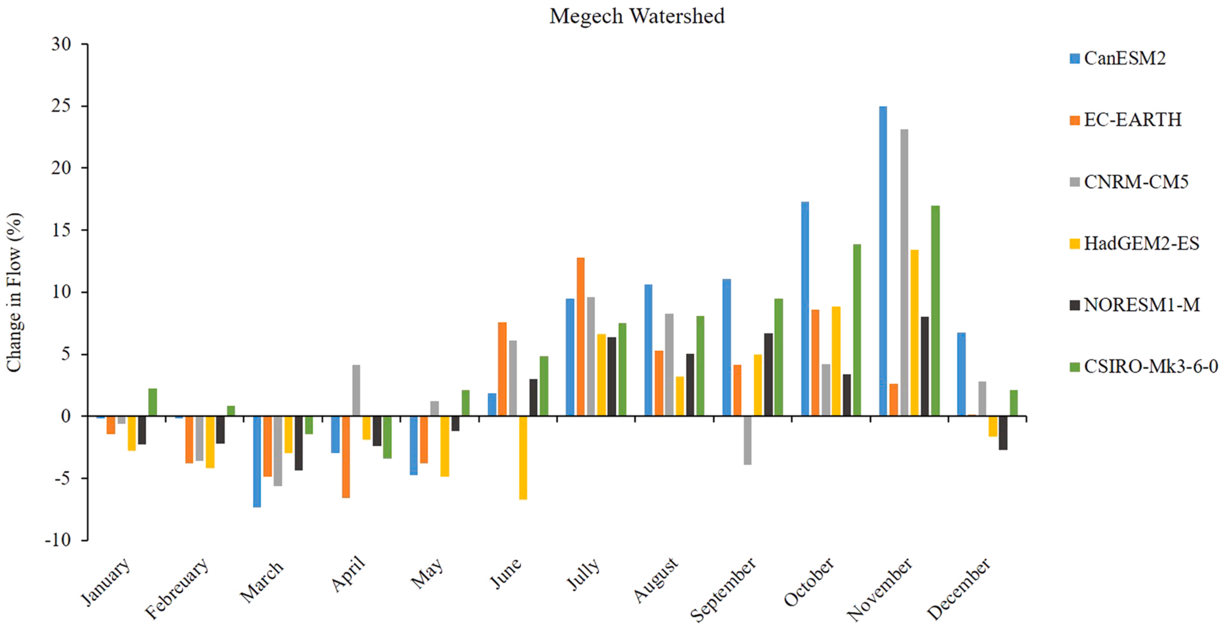

Fig. 13. Change in stream flow in Megech watershed.

climate models in all months, the change in the Ribb watershed showed a similar change pattern in time compared to the Gumara watershed. This similarity is because the two watersheds shared the same meteorological stations in simulations of the hydrological model. The increment of streamflow in the watershed was also verified by other studies conducted in the region (Wagena et al., 2016; Yimer et al., 2009).

In the Megech watershed, the streamflow was projected and the change showed increasing in the summer and autumn seasons in the last thirty years of this century under all climate models except CRNM-CM5 which showed a decreasing trend in September. Compared to other watersheds, the lowest maximum change in streamflow was predicted (24.97 m^3/s) in this watershed. In the region, the maximum temperature was observed in the winter and spring seasons, indicating that much of the rainfall is changed to evapotranspiration and the flow is predicted to decrease like other studies (Gleick, 1987; Karl and Riebsame, 1989; Wigley and Jones, 1985).

The maximum decreasing value of change in streamflow (−7.371%) is predicted in March under the CanESM2 climate model (Fig. 13).

Besides to predicting the change in streamflow because of climate change in a monthly basis, the annual mean streamflow change between the baseline period and the last thirty years of this century is also evaluated. The annual mean streamflow in all watersheds under all climate models ranges from 1% to 6.43%. The maximum annual average change in streamflow was predicted in the Ribb watershed under CSIRO-Mk3–6–0, and the minimum change was forecasted in the Megech watershed under HadGEM2-ES. Unlike other climate models, the change in annual average streamflow under HadGEM2-ES in the Gilgel Abay watershed was predicted to decrease by 1.39% in the last thirty years of this century. As far as the four watersheds shared the same meteorological stations in the simulation process, the variation of change in streamflow on an annual average basis especially between the Gumara and Ribb watersheds was negligible. As it is shown in (Fig. 14), the two lines nearly overlapped especially in three climate models (EC-EARTH, CNRM-CM5, and HadGEM2-ES).

4. Conclusion

This study revealed that, under all climate models, the climate is changing and it is altering the flow conditions of watersheds in the Lake Tana basin. Despite this finding, the change in temperature and precipitation does not show consistent variability in all used climate model outputs, especially temperature showed an increasing trend in the highest emission scenario (RCP 8.5), over the last thirty years of this century. The highest annual mean temperature is likely to be increasing by 4.15 °C under the CSIRO-Mk3–6–0 climate model relative to other models used in this study, whereas the lowest change is expected under the EC-EARTH climate model. Even though the change in precipitation seems insignificant, seasonally, it showed considerable variabilities due to this high emission scenario.

The change in climate potentially increases the streamflow of the four watersheds during the rainy (summer) and autumn seasons. The highest change in stream flow is expected to be observed in November in all watersheds. Due to the increment of temperature being very high in the winter and spring seasons, the potential evapotranspiration is likely to be increasing in the basin. Furthermore, rainfall is not usually common in the winter and spring seasons in the region and even the change in rainfall showed a negative change under most climate models. Thus, the increment of potential evapotranspiration and reduction of rainfall is likely to cause a decreasing of stream flow in the dry seasons.

Generally, the study showed that future climate change is expected to potentially alter the streamflow conditions, especially in the two extreme flow cases of watersheds, and therefore, any water management project plans should consider the future stream flow dynamics caused by climate change. Finally, based on the result of this study, appropriate physical and biological soil and water conservation measures are highly recommended to protect against flooding, soil erosion, and sedimentation of the lake, and hydrological drought in the basin.

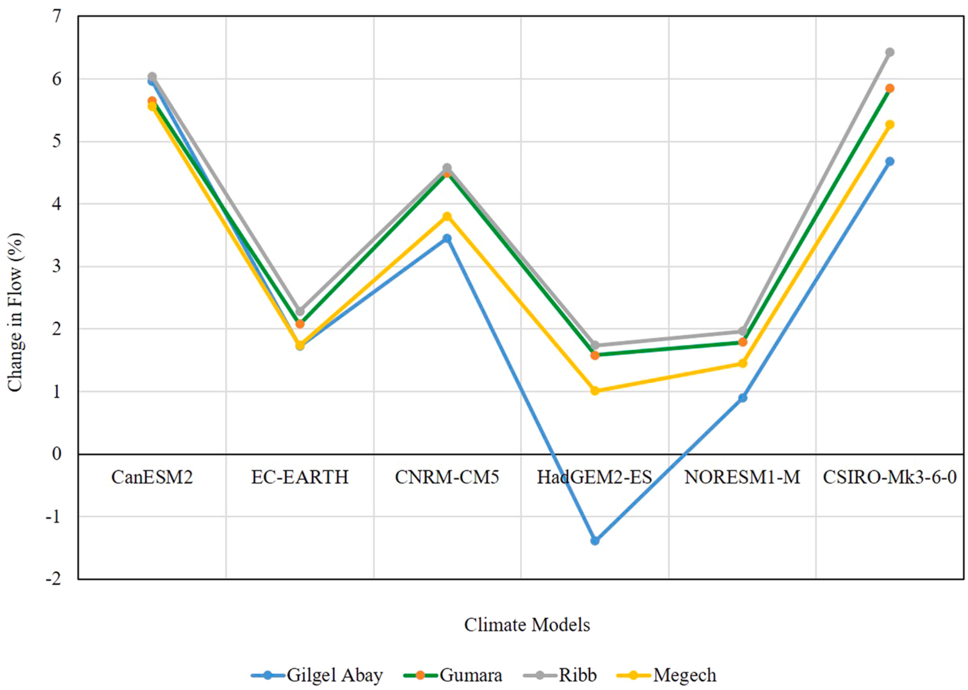

Fig. 14. Change in flow of watersheds in Lake Tana basin.

CRediT authorship contribution statement

Gashaw Gismu Chakilu: Designed the hydrological model calibration and validation, Downscaling of climate data, Writing of the paper, Revising the manuscript. **Szegedi Sándor, Túri Zoltán**: Supervised the research, Edited the paper, Revised the manuscript. **Kwanele Phinzi**: Has also edited, Revised the manuscript. All authors have read and agreed to the revised version of the manuscript.

Declaration of Competing Interest

The authors declare that they have no known competing financial interests or personal relationships that could have appeared to influence the work reported in this paper.

Acknowledgments

We would like to thank the National Meteorological Agency of Ethiopia (NMA), and Ministry of Water and Energy (MoWE) of Ethiopia for providing free input data for this research work. This paper is part of a PhD research project of the first author (G.G.C.) funded by the Tempus Public Foundation (Hungary) within the framework of the Stipendium Hungaricum Scholarship Programme, supported by Ministry of Education (MoE) of Ethiopia and Debark University.

References

Adem, A.A., Melesse, A.M., Tilahun, S.A., Setegn, S.G., Ayana, E.K., Wale, A., Assefa, T.T., 2014. Climate change projections in the upper Gilgel Abay River catchment, Blue Nile basin Ethiopia. Nile river Basin. Springer, pp. 363–388.

Allen, R.G., Pereira, L.S., Raes, D., & Smith, M., 1998, Chapter 2 FAO Penman-Monteith equation. Crop Evapotranspiration-Guidelines for Computing Crop Water Requirements. FAO Irrigation and Drainage Paper, 56.

Ayele, H.S., Li, M.-H., Tung, C.-P., 2016. Assessing Climate Change Impact on Gilgel Abbay and Gumara Watershed Hydrology, the Upper Blue Nile Basin, Ethiopia. Terr., Atmos. Ocean. Sci. 27 (6).

Bekele, W.T., Haile, A.T., Rientjes, T., 2021. Impact of climate change on the streamflow of the Arjo-Didessa catchment under RCP scenarios. J. Water Clim. Change 12 (6), 2325–2337. https://doi.org/10.2166/wcc.2021.307.

Chakilu, Gashaw G., Moges, M.A., 2017. Assessing the land use/cover dynamics and its impact on the Low Flow of Gumara Watershed, Upper Blue Nile Basin, Ethiopia. Hydrol.: Curr. Res. 08 (01), 1–6. https://doi.org/10.4172/2157-7587.1000268.

Chakilu, Gashaw Gismu, Sándor, S., Zoltán, T., 2020. Change in stream flow of gumara watershed, upper blue nile basin, ethiopia under representative concentration pathway climate change scenarios. Water (Switz.) 12 (11), 1–14. https://doi.org/10.3390/w12113046.

Conway, D., Schipper, E.L.F., 2011. Adaptation to climate change in Africa: Challenges and opportunities identified from Ethiopia. Glob. Environ. Change 21 (1), 227–237.

Dams, J., Woldeamlak, S.T., Batelaan, O., 2008. Predicting land-use change and its impact on the groundwater system of the Kleine Nete catchment, Belgium. Hydrol. Earth Syst. Sci. 12 (6), 1369–1385.

Fang, G.H., Yang, J., Chen, Y.N., Zammit, C., 2015. Comparing bias correction methods in downscaling meteorological variables for a hydrologic impact study in an arid area in China. Hydrol. Earth Syst. Sci. 19 (6), 2547–2559. https://doi.org/10.5194/hess-19-2547-2015.

FAO, 2010, Manual on small earth dams. Report: FAO Irrigation and Drainage Paper 64, 64, 18. ⟨http://scholar.google.com/scholar?hl=en&btnG=Search&q=intitle:Manual+on+small+earth+dams#2⟩.

FAO, & UNESCO, 1977, FAO-UNESCO soil map of the world, 1:5000000. Africa. Fao Soil Bulletin, VI(1), 346.

Fulco Ludwig, Catharien Terwisscha van Scheltinga, Jan Verhagen, Bart Kruijt, Ekko van Ierland, Rob Dellink, Karianne de Bruin, K. de B. and P. K. (2007). Policy Department Economic and Scientific Policy - Climate change impacts on Developing Countries - EU Accountability. Public Health, January 2007, 1–45. https://www.europarl.europa.eu/RegData/etudes/etudes/join/2007/393511/IPOL-ENVI_ET(2007)393511_EN.pdf.

Gebrehiwot, S.G., Taye, A., Bishop, K., 2010. Forest cover and stream flow in a headwater of the Blue Nile: complementing observational data analysis with community perception. Ambio 39 (4), 284–294.

Gebremicael, T.G., Mohamed, Y.A., Betrie, G.D., Van der Zaag, P., Teferi, E., 2013. Trend analysis of runoff and sediment fluxes in the Upper Blue Nile basin: A combined analysis of statistical tests, physically-based models and landuse maps. J. Hydrol. 482, 57–68.

Gleick, P.H., 1987. Regional hydrologic consequences of increases in atmospheric CO 2 and other trace gases. Clim. Change 10 (2), 137–160.

Gupta, H.V., Sorooshian, S., Yapo, P.O., 1999. Status of automatic calibration for hydrologic models: Comparison with multilevel expert calibration. J. Hydrol. Eng. 4 (2), 135–143.

Haile, A.T., Akawka, A.L., Berhanu, B., Rientjes, T., 2017. Changes in water availability in the Upper Blue Nile basin under the representative concentration pathways scenario. Hydrol. Sci. J. 62 (13), 2139–2149. https://doi.org/10.1080/02626667.2017.1365149.

Haregeweyn, N., Melesse, B., Tsunekawa, A., Tsubo, M., Meshesha, D., Balana, B.B., 2012. Reservoir sedimentation and its mitigating strategies: a case study of Angereb reservoir (NW Ethiopia). J. Soils Sediment. 12 (2), 291–305.

Hayhoe, K., Edmonds, J., Kopp, R.E., LeGrande, A.N., Sanderson, B.M., Wehner, M.F., Wuebbles, J., 2017. Climate models, scenarios, and projections. *Climate Science Special Report: Fourth National Climate*. Assess., I 133–160. https://doi.org/10.7930/J0WH2N54.U.S.

Henderson, P.R.M., & Reinert, S.A., 2016, P O L I N a D E K H T Y a R a M R a M M I G D a L. Mba 2016. ⟨www.hbsp.harvard.edu⟩.

Ho, C.K., Stephenson, D.B., Collins, M., Ferro, C.A.T., Brown, S.J., 2012. Calibration strategies: a source of additional uncertainty in climate change projections. Bull. Am. Meteorol. Soc. 93 (1), 21–26.

IPCC, 2014, Intergovernmental p Panel on Climate Change: Sythesis Report. In Managing the Risks of Extreme Events and Disasters to Advance Climate Change Adaptation: Special Report of the Intergovernmental Panel on Climate Change (Vol. 9781107025). ⟨https://doi.org/10.1017/CBO9781139177245.003⟩.

IPCC, 2018, Global warming of 1.5°C. In Global Warming of 1.5°C. An IPCC Special Report on the impacts of global warming of 1.5°C above pre-industrial levels and related global greenhouse gas emission pathways, in the context of strengthening the global response to the threat of climate change, sustainable development, and efforts to eradicate poverty. ⟨https://doi.org/10.1017/9781009157940⟩.

Karl, T.R., Riebsame, W.E., 1989. The impact of decadal fluctuations in mean precipitation and temperature on runoff: a sensitivity study over the United States. Clim. Change 15 (3), 423–447.

Kim, U., Kaluarachchi, J.J., 2009. Climate change impacts on water resources in the upper Blue Nile River Basin, Ethiopia. J. Am. Water Resour. Assoc. Vol. 45 (Issue 6) https://doi.org/10.1111/j.1752-1688.2009.00369.x.

Malede, D.A., Agumassie, T.A., Kosgei, J.R., Andualem, T.G., Diallo, I., 2022. Recent Approaches to Climate Change Impacts on Hydrological Extremes in the Upper Blue Nile Basin, Ethiopia. Earth Syst. Environ. https://doi.org/10.1007/s41748-021-00287-6.

Mekonnen, D.F., Duan, Z., Rientjes, T., Disse, M., 2018. Analysis of combined and isolated effects of land-use and land-cover changes and climate change on the upper Blue Nile River basin's streamflow. Hydrol. Earth Syst. Sci. 22 (12), 6187–6207.

Mena, M.M., 2018. Community Adoption of Watershed Management Practices at Kindo Didaye District, Southern Ethiopia. Int. J. Environ. Sci. Nat. Resour. 14 (2) https://doi.org/10.19080/ijesnr.2018.14.555881.

Mengistu, D., Bewket, W., Dosio, A., Panitz, H.-J., 2021. Climate change impacts on water resources in the Upper Blue Nile (Abay) River Basin, Ethiopia. J. Hydrol. 592, 125614.

Mulat, A.G., Moges, S.A., 2014. Assessment of the Impact of the Grand Ethiopian Renaissance Dam on the Performance of the High Aswan Dam. J. Water Resour. Prot. 06 (06), 583–598. https://doi.org/10.4236/jwarp.2014.66057.

Nash, J.E., Sutcliffe, J.V., 1970. River flow forecasting through conceptual models part I—A discussion of principles. J. Hydrol. 10 (3), 282–290.

Neitsch, S.L., Arnold, J.G., Kiniry, J.R., Srinivasan, R., & Williams, J.R. (2002). Soil and Water Assessment Tool User's Manual. *TWRI Report TR-192*, 412. ⟨http://swat.tamu.edu/media/1294/swatuserman.pdf⟩.

North, G.R., 2014. Global climate change. A World Clim. Change Cult. -Shift April, 25–42. https://doi.org/10.1007/978-94-007-7353-0_3.

Poveda, A.C., Martínez, C.I.P., 2011. Trends in economic growth, poverty and energy in Colombia: Long-run and short-run effects. Energy Syst. 2 (3–4), 281–298. https://doi.org/10.1007/s12667-011-0036-7.

Power, S.B., Delage, F., Colman, R., Moise, A., 2012. Consensus on twenty-first-century rainfall projections in climate models more widespread than previously thought. J. Clim. 25 (11), 3792–3809. https://doi.org/10.1175/JCLI-D-11-00354.1.

Rathjens, H., Bieger, K., Srinivasan, R., & Arnold, J.G., 2016, CMhyd User Manual Documentation for preparing simulated climate change data for hydrologic impact studies. p.16p.

Rientjes, T.H.M., Haile, A.T., Kebede, E., Mannaerts, C.M.M., Habib, E., Steenhuis, T.S., 2011. Changes in land cover, rainfall and stream flow in Upper Gilgel Abbay catchment, Blue Nile basin–Ethiopia. Hydrol. Earth Syst. Sci. 15 (6), 1979–1989.

Roth, V., Lemann, T., Zeleke, G., Subhatu, A.T., Nigussie, T.K., Hurni, H., 2018. Effects of climate change on water resources in the upper Blue Nile Basin of Ethiopia. Heliyon 4 (9). https://doi.org/10.1016/j.heliyon.2018.e00771.

Schaller, N., Mahlstein, I., Cermak, J., Knutti, R., 2011. Analyzing precipitation projections: A comparison of different approaches to climate model evaluation. J. Geophys. Res. Atmospheres 116 (10). https://doi.org/10.1029/2010JD014963.

Seager, R., Ting, M., Held, I., Kushnir, Y., Lu, J., Vecchi, G., Huang, H.-P., Harnik, N., Leetmaa, A., Lau, N.-C., Li, C., Velez, J., Naik, N., 2007. Model projections of an imminent transition to a more arid climate in southwestern North America. Sci. (N. Y., N. Y.) 316 (5828), 1181–1184. https://doi.org/10.1126/science.1139601.

Setegn, Shimelis G., Rayner, D., Melesse, A.M., Dargahi, B., Srinivasan, R., 2011. Impact of climate change on the hydroclimatology of Lake Tana Basin, Ethiopia. Water Resour. Res. 47 (4), 1–13. https://doi.org/10.1029/2010WR009248.

Setegn, Shimelis G., Srinivasan, R., Dargahi, B., 2008. Hydrological modelling in the Lake Tana Basin, Ethiopia using SWAT model. Open Hydrol. J. 2 (1).

Setegn, Shimelis Gebriye, 2010, Modelling hydrological and hydrodynamic processes in lake Tana basin, Ethiopia. KTH.

Shao, G., Guan, Y., Zhang, D., Yu, B., Zhu, J., 2018. The impacts of climate variability and land use change on streamflow in the Hailiutu river basin. Water 10 (6), 814.

Sivakumar, B., 2011. Global climate change and its impacts on water resources planning and management: Assessment and challenges. Stoch. Environ. Res. Risk Assess. 25 (4), 583–600. https://doi.org/10.1007/s00477-010-0423-y.

Stocker, T.F., Qin, D., Plattner, G.K., Tignor, M.M.B., Allen, S.K., Boschung, J., Nauels, A., Xia, Y., Bex, V., Midgley, P.M., 2013. Climate change 2013 the physical science basis: Working Group I contribution to the fifth assessment report of the intergovernmental panel on climate change. Clim. Change 2013 Phys. Sci. Basis: Work. Group I Contrib. Fifth Assess. Rep. Intergov. Panel Clim. Change 9781107057, 1–1535. https://doi.org/10.1017/CBO9781107415324.

Stoll, S., Hendricks Franssen, H.J., Butts, M., Kinzelbach, W., 2011. Analysis of the impact of climate change on groundwater related hydrological fluxes: A multi-model approach including different downscaling methods. Hydrol. Earth Syst. Sci. 15 (1), 21–38. https://doi.org/10.5194/hess-15-21-2011.

Suppiah, R., Collier, M., Jeffrey, S., Rotstayn, L., Syktus, J., Wong, K., 2013. Simulated and projected summer rainfall in tropical Australia: Links to atmospheric circulation using the CSIRO-Mk3.6 climate model. Aust. Meteorol. Oceanogr. J. 63 (1), 15–26. https://doi.org/10.22499/2.6301.002.

Tebaldi, C., Arblaster, J.M., Knutti, R., 2011. Mapping model agreement on future climate projections. Geophys. Res. Lett. 38 (23), 1–5. https://doi.org/10.1029/2011GL049863.

Terink, W., Hurkmans, R., Torfs, P., Uijlenhoet, R., 2010. Evaluation of a bias correction method applied to downscaled precipitation and temperature reanalysis data for the Rhine basin. Hydrol. Earth Syst. Sci. 14 (4), 687–703.

Tesemma, Z.K., Mohamed, Y.A., Steenhuis, T.S., 2010. Trends in rainfall and runoff in the Blue Nile Basin: 1964–2003. Hydrol. Process. 24 (25), 3747–3758.

Teutschbein, C., Seibert, J., 2012. Bias correction of regional climate model simulations for hydrological climate-change impact studies: Review and evaluation of different methods. J. Hydrol. 456, 12–29.

Tigabu, T.B., Wagner, P.D., Hörmann, G., Kiesel, J., Fohrer, N., 2021. Climate change impacts on the water and groundwater resources of the lake tana basin, ethiopia. J. Water Clim. Change 12 (5), 1544–1563. https://doi.org/10.2166/wcc.2020.126.

US EPA, 2016, Climate change indicators in the United States 2016 Fourth Edition. Climate Change Indicators in the United States: 2016, 663–670. ⟨http://www.epa.gov/climate-indicators%0Awww.epa.gov/climate-indicators⟩.

Wagena, M.B., Sommerlot, A., Abiy, A.Z., Collick, A.S., Langan, S., Fuka, D.R., Easton, Z.M., 2016. Climate change in the Blue Nile Basin Ethiopia: implications for water resources and sediment transport. Clim. Change 139 (2), 229–243. https://doi.org/10.1007/s10584-016-1785-z.

Wigley, T.M.L., Jones, P.D., 1985. Influences of precipitation changes and direct CO 2 effects on streamflow. Nature 314 (6007), 149–152.

Worqlul, A.W., Dile, Y.T., Ayana, E.K., Jeong, J., Adem, A.A., Gerik, T., 2018. Impact of climate change on streamflow hydrology in headwater catchments of the Upper Blue Nile Basin, Ethiopia. Water 10 (2), 120.

Yihdego, Y., Webb, J., 2013. An empirical water budget model as a tool to identify the impact of land-use change in stream flow in southeastern Australia. Water Resour. Manag. 27 (14), 4941–4958.

Yimer, G., Jonoski, A., Griensven, A.V., 2009. Hydrological response of a catchment to climate change in the upper Beles river basin, upper blue Nile, Ethiopia. Nile Basin Water Eng. Sci. Mag. 2 (1), 49–59.

Zhang, Y.-K., Schilling, K.E., 2006. Effects of land cover on water table, soil moisture, evapotranspiration, and groundwater recharge: a field observation and analysis. J. Hydrol. 319 (1–4), 328–338.